Arabian Journal of Geosciences (2020) 13:858
https://doi.org/10.1007/s12517-020-05750-8

ORIGINAL PAPER

Petrographic and rare earth elemental characteristics of Cambrian *Girvanella* oncoids exposed in the North China Platform: Constraints on forming mechanism, REE sources, and paleoenvironments

Muhammad Riaz[1,2,3] · Tehseen Zafar[4] · Khalid Latif[5,6] · Shahid Ghazi[3] · Enzhao Xiao[6]

Received: 25 January 2020 / Accepted: 16 July 2020

Abstract

Oncoid-bearing Mioalingian strata in the North China Platform represent late highstand/forced regressive systems tract(s). In the current study, sequence stratigraphy, sedimentology, and microscopic studies were carried out to interpret the forming mechanism and paleoenvironment of these oncoids. Microscopic studies show the typical distribution of filamentous cyanobacteria (*Girvanella*) in the Cambrian oncoids. Based on these observations, the oncoids can be classified into three kinds, i.e., *Girvanella*-core oncoids, *Girvanella*-cortex oncoids, and *Girvanella*-full oncoids. Furthermore, the studied oncoids hold pyrite crystals and dolomite minerals that also indicate the influence of sulfate-reducing bacteria on their formation. The presence of *Girvanella*, pyrite, and dolomite in the cores and cortices of these distinctive oncoids depicts its microbial origin that flourished under relatively high-energy settings. The present work offers a reference example for the involvement of microbes, particularly *Girvanella*, in the development of microbial carbonates in the North China carbonate platform during the Cambrian period. Geochemistry of the Cambrian oncoids is interpreted in order to determine the involvement of detrital fractions, sources of rare earth elements (REEs), and paleoenvironmental settings. The results of slightly negative Eu anomalies, higher La/Yb (6.8–15.1), and the larger Y/Ho variations (30.17–42.08) in the studied oncoids advocate that these oncoids have been subjected to terrigenous input during their formation. Considering the absence of Ce anomaly, Gd/Gd* ratios (< 1), and lesser values of Y/Ho (30.17–33.93), we propose that these oncoids have been influenced by diagenetic activities. Relatively greater values of Er/Nd (0.09–0.23) suggest seawater signature preserved by the marine sediments. Meanwhile, observed weak negative Eu anomalies within the oncoids point out the retention of the original marine water characteristics, whereas lower values of the Y/Ho propose freshwater participation from the rivers in the seawater during precipitation of oncoids. Based on the ratios Er/Nd, $(Nd/Yb)_N$, La/Yb, and depletion and variation of REEs, it can be confirmed that the sources of these REEs within the Cambrian oncoids are mainly from terrigenous input. However, the higher Er/Nd ratios are sourced from marine carbonates. Relatively lower values of Mo/U (1.10–2.46), V/Cr (< 2), V/(V + Ni) ratios (0.24–0.33), and deficiency of Ce anomaly in studied oncoids suggest their development under oxic environments. In addition, the variation of Sr/Cu (42–54) and Sr/Ba (35–79) indicates their growth under arid climatic conditions and classic marine settings. Considering these geochemical signatures, it can be concluded that the oncoids of the North China Platform flourished under oxic, arid, and classic marine conditions.

Keywords *Girvanella* · Microbial mat · Trace and rare earth elements · Cambrian (Miaolingian) oncoids · China

Responsible Editor: Santanu Banerjee

Electronic supplementary material The online version of this article (https://doi.org/10.1007/s12517-020-05750-8) contains supplementary material, which is available to authorized users.

✉ Tehseen Zafar
zafar@vip.gyig.ac.cn

Muhammad Riaz
riazjass@yahoo.com

Khalid Latif
khlatif@yahoo.com

Shahid Ghazi
ghazigeo6@yahoo.com

Back Affiliation

Published online: 26 August 2020

Introduction

Oncoids (> 2 mm in diameter) are generally considered as rounded forms that comprise of nuclei of varying grain types and cortices composed of entirely or a combination of calcified microbes (Riding 1991; Hanken et al. 2015; Mei et al. 2019a, b; Xiao et al. 2020a, b). The oncoid usually exhibits dual nature: (1) oncoids possess the mobile attribute of coated grain that has an irregular and uneven surface and are generally considered microbial in origin (Liu and Zhang 2012; Xiao et al. 2020a, b), which is distinctive from ooids whose origin is debatable (Duguid et al. 2010; Diaz and Eberli 2019), and (2) oncoids also represent biosedimentary structures, such as stromatolite, which has successive laminations around the core (Riding 2011a, b).

Oncoids are the major component of carbonates that flourished in various environments in the entire chronostratigraphic column such as (1) lacustrine and shallow water environments in the early Cambrian (Schaefer et al. 2001), (2) fluviatile to lacustrine environments in the middle Cambrian to Jurassic (Olivier et al. 2004; Brigaud et al. 2009; Zhang et al. 2014a, b; Xiao et al. 2020a, b), and (3) lacustrine, riverine, and tidal flat environments of the shallow sea in the recent (Jones 1992; Zhang et al. 2013). According to various depositional environments, the origin of oncoids can be interpreted as (1) sophisticated metabolic mechanisms within microbial mats, (2) microbially mediated calcium carbonate precipitation, and (3) formation of particles via trapping and binding in a marine environment (Dahanayake 1977; Peryt 1981; Flügel and Munnecke 2010; Jones and Renaut 2010; Jones 2011; Zhang et al. 2014a, b; Han et al. 2015; Zhang et al. 2015a, b; Qi et al. 2016; Mei et al. 2019a, b). The evolutionary study of ancient oncoids is significant to interpret fluctuations in depositional conditions as well as control of microbial activities on the forming mechanism of oncoids. Hence, the studies of oncoids from the ancient strata are important clues to restore paleoclimate, paleoenvironment, sea-level fluctuations, and sedimentary environment (Vedrine et al. 2007; Zhou et al. 2017; Xiao et al. 2020a, b).

Several researchers studied the Cambrian oncoids of the North and South China to highlight its various aspects such as classification, forming environment, textural composition, growth mechanism and controlling factors (Yang et al. 2011), mass-occurrence (anoxic) event of oncoids (Zhang et al. 2014b, 2015a), the ultra-fabrics and biomineralization of oncoids (Zhang et al. 2014a), forming mechanism of oncoids (Han et al. 2015), coupling variation of oncoids (Zhang et al. 2015b), formation of oncoids via microbial activities (Wang and Xiao 2018; Mei et al. 2019a, b); and the various shape of oncoids and their paleoenvironmental conditions (Xiao et al. 2020a, b). However, a study on the involvement of microbes particularly *Girvanella* in different parts of Cambrian oncoids is quite insufficient. Moreover, geochemistry of the *Girvanella* oncoids regarding the involvement of detrital fractions, sources of rare earth elements (REEs) in these oncoids, and paleoenvironmental settings are still unresolved. The present study describes the *Girvanella* oncoids, its different forms, and the influence of cyanobacteria in the formation of oncoids in the Miaolingian strata of the North China Platform (NCP). In addition, current research highlights that these oncoids have been subjected to terrigenous input and diagenetic activities during their formation.

Geological background

The tectonic history of China delineates the development of main tectonic blocks including Tarim, North China, and South China (Zheng et al. 2013; Myrow et al. 2015) (Fig. 1a, b). The studied NCP was developed in the tropical to subtropical regions of the Sino-Korean Block, close to Australia, in the early Paleozoic time (Wotte et al. 2007) (Fig. 1a). It is restricted by main suture zones on the north and south by Hinggan Fold Belt and Qinling Dabieshan Belt, respectively (Myrow et al. 2015) (Fig. 1b), whereas it is bounded by east and west with Tanlu Fault and Helan aulacogen, accordingly (Zheng et al. 2013; Myrow et al. 2015) (Fig. 1b). Deposition of the Cambrian sediments in the NCP initiated approximately in late Series 2 with a sea-level rise that deposited Cambrian strata on it as shown in Fig. 1c (see Mei 1996, 2011; Riaz et al. 2019a, b). The Cambrian strata overlap with the Precambrian strata in this widespread carbonate platform in a similar pattern as described in North America (e.g., Peters and Gaines 2012). Consequently, Cambrian succession with the thickness of 700 m was developed on the NCP, which can approximately be divided into three successions in ascending order (Meng et al. 1997; Mei 1996, 2011; Riaz et al. 2019a, b) (Fig. 1c): (1) a mixed rock unit of the Series 2, which is composed of red beds (i.e., dolostone) and carbonate rocks (i.e., limestone), (2) carbonate strata of the Miaolingian predominated by oolitic grainstones along with the minor amount of oncolites at some places, and (3) carbonate succession of the Furongian that mainly comprises carbonate muds. These rock units delineate characteristic cyclicity that helps in further classifying them into nine third-order sequences (from DS_1 to DS_9) as shown in Fig. 1c. The sequence boundaries of the Cambrian strata can be marked by punctuated surfaces and drowning unconformities (Fig. 1c).

According to the new chronostratigraphic division (Peng and Zhao 2018; Mei et al. 2020a), the studied Miaolingian strata consist of the Maozhuang, Xuzhuang, Zhangxia, and Gushan formations that deposited in four third-order depositional sequences (DS_3 to DS_6 in Fig. 1c). The Maozhuang Formation and the lower part of the Xuzhuang Formation comprise a succession of a tidal-flat depositional system marked by carbonate rocks with the intergrowth of red beds (Fig. 1c). Thick-bedded massive oolitic grainstones along with the minor amount of oncolites are commonly

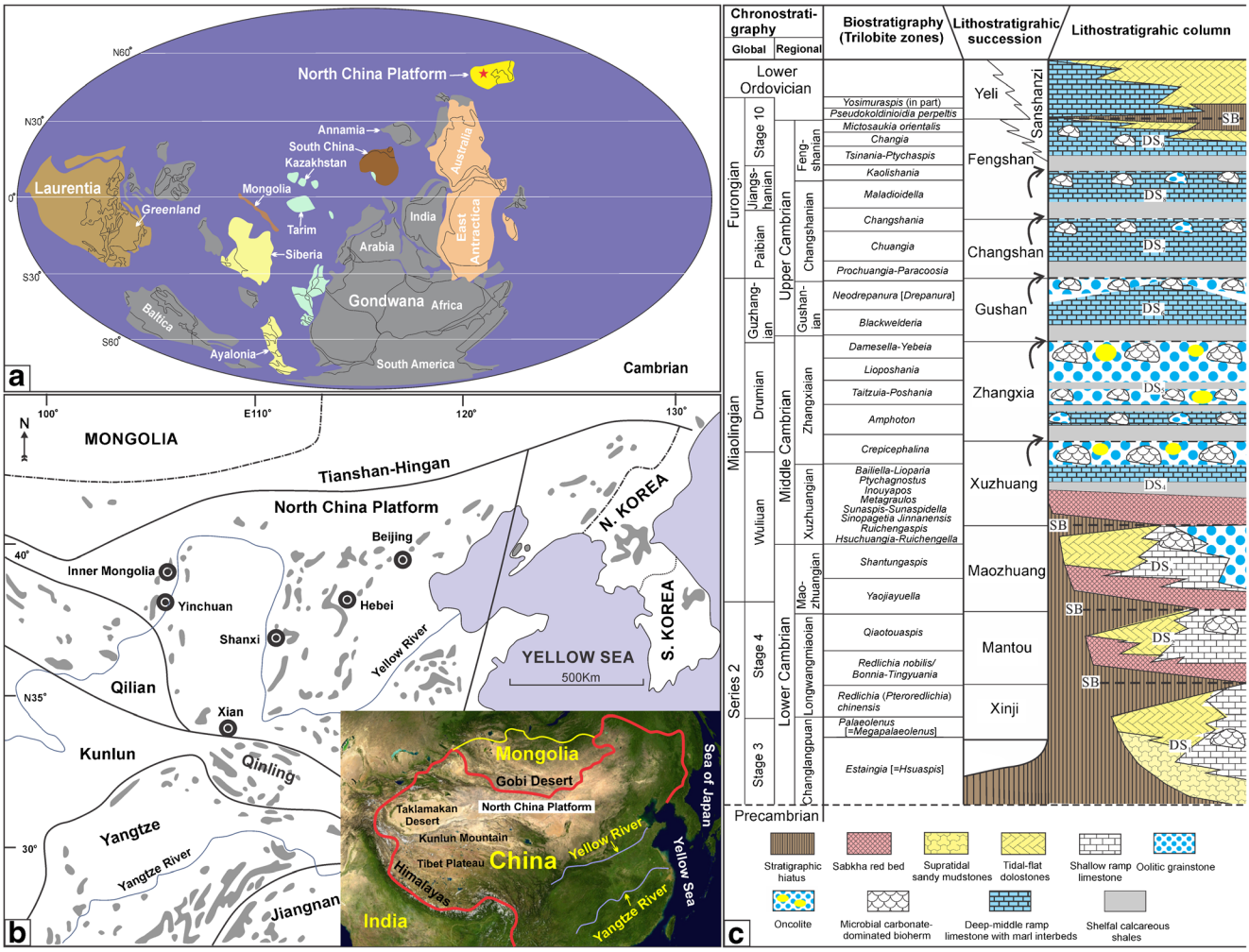

Fig. 1 **a** Global location of the North China Platform (NCP). **b** Map showing the geological framework of the NCP (modified after Riaz et al. 2019a, b). Gray regions show the exposed Cambrian strata. Inset satellite image (lower right corner) showing the NCP in a regional perspective. **c** The sedimentary succession of the Cambrian strata (from DS_1 to DS_9) in the NCP (modified after Mei et al. 2020a)

concentrated in the upper parts of the Xuzhuang, Zhangxia, and Gushan formations (DS_4 to DS_6 in Fig. 1c), which constitute the time-specific facies (Brett et al. 2012; Schinder 2012). These deposits develop in both highstand and forced regressive systems that fulfill the forced regressive model proposed in several previous studies (i.e., Helland-Hansen and Gjelberg 1994; Schlager and Warrlich 2009; Mei 2010; Samanta et al. 2016). During each depositional period of FRSTs of the Miaolingian strata (DS_4 to DS_6), a broad oolitic shoal developed in the NCP that represents a carbonate platform dominated by ooidal sands (Pratt et al. 2012).

Materials and methods

Extensive geological fieldwork has been carried out in the NCP. Macroscopic features associated with oncoids are examined in the upper part of the Cambrian (Miaolingian) Xuzhuang and Zhangxia formations (Fig. 2a–h). The oncoids of the Xuzhuang Formation are irregular and rounded in shape without clear separation of cores and cortices (Fig. 2b, d), whereas the Zhangxia Formation comprises of of elongated and elliptical to spheroidal shape oncoids with definite cores and successively repeated laminations in their cortices similar to stromatolites (Fig. 2f, h). These formations have conformable upper and lower contacts with Cambrian Miaolingian strata; however, at places, the Xuzhuang Formation has unconformable lower contact with Precambrian strata (Fig. 2a, g). A petrographic analysis of 360 carbonates samples from the targeted bed was carried out. Detailed investigation of microfacies was conducted in order to understand the microscopic composition and fabric of the formation, the structure of oncoids, its various types, and the presence of microbes particularly cyanobacteria as well as grains other than oncoids. Thin sections were observed under a high-magnification petrographic microscope at the China University of Geosciences, Beijing (CUGB). Photomicrographs for the high-resolution examination of oncoids were captured with a camera attached

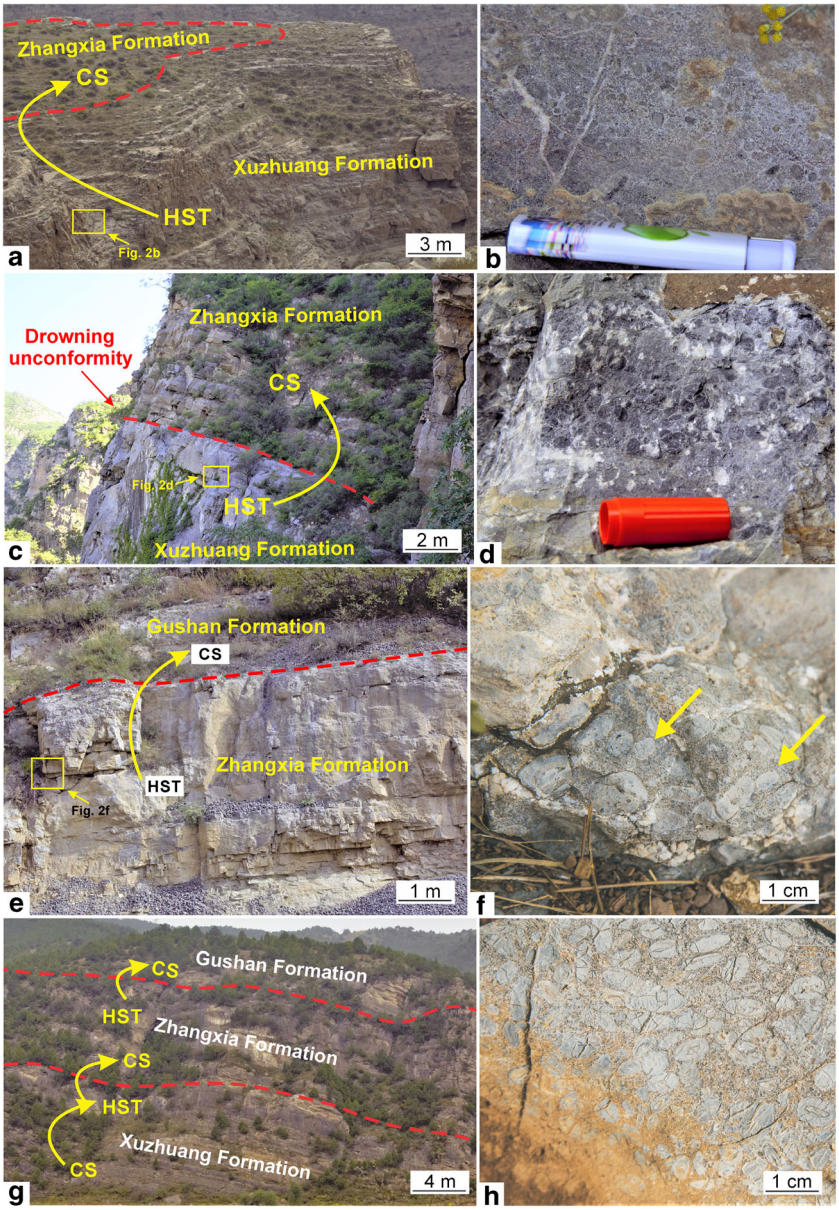

Fig. 2 Important sequence boundaries, sedimentary features of the Miaolingian strata and locations of oncoids in the various region of the North China Platform (NCP). **a** The Xuzhuang Formation having massive oolitic limestone along with oncolite, conformably overlain by the Zhangxia Formation. **b** Irregular oncolite in the Xuzhunag Formation. **c** Drowning unconformity separates the Miaolingian strata. **d** Rounded oncolite in the Xuzhunag Formation. **e** The contact between Zhangxia and Gushan formations. **f** Elongated oncolite in the Zhangxia Formation. **g** Division of entire Cambrian Miaolingian strata. **h** Elliptical to spheroidal oncolite with dominant core in the Zhangxia Formation

to the petrographic microscope. CorelDraw graphic software was used to construct different figures and collage of different photomicrographs used in the current study.

Additionally, geochemical data, i.e., inductively coupled plasma–mass spectrometry (ICP–MS), was adopted from Xiao et al. (2020a) to determine the exact sources of REEs and paleoenvironmental conditions of *Girvanella* oncoids. The results of the geochemical data are presented in Supplementary Table 1.

Petrography of oncoids

Oncoids are mostly elliptical to spheroidal in shape under the microscope. The shape of oncoids is controlled by the shape of core and concentric laminae. These oncoids were classified into three varieties: *Girvanella*-core oncoids, *Girvanella*-cortex oncoids, and *Girvanella*-full oncoids based on texture and outline of the cortex. The detail descriptions of these oncoids are given below.

Girvanella-core oncoids

Description These oncoids are typically > 1.5 mm in diameter and surrounded by sparite cement (Fig. 3a–c). These oncoids have a well-developed core of *Girvanella* and cortex of dolomite (Fig. 3a–c). These oncoids (Fig. 3a, b) are similar to superficial ooids that have a thick core and thin cortex. The cortices of the oncoids are associated with crystals of dolomite that range in size from 100 to 150 μm (Fig. 3a–c). Moreover,

pyrite grains are observed within and the surrounding areas of the oncoids. Further observation shows the minor amount of bioclasts (brachiopods and/or trilobites) and patches of micrite (possibly *Girvanella*) in the surrounding region of the oncoids (Fig. 3a).

Interpretation Sparite cement and presence of brachiopods and/or trilobites indicate the high-energy setting of these oncoids (Flügel 2004). The superficial shape of oncoids indicates its migration from low- to high-energy conditions (Riaz et al. 2019b). The cortices of these oncoids are thick indicating more life span in a high-energy environment (Riaz 2019). Furthermore, the cortex is associated with crystals of dolomite that possibly formed by capillary condensation due to fluctuation of relative sea-level (Guo et al. 2020). The dolomite is genetically associated with extracellular polymeric substance (EPS) degradation that forms cyanobacteria-dominated microbial mat (Decho and Gutierrez 2017). In the process, the elimination of EPSs occurred through both active and passive mineralization that produces Mg^{2+} ions, which is captured by *in vivo* EPSs. Further pyrite crystals in the surrounding area of the oncoids represent the metabolize products of sulfate-reducing bacteria in cyanobacterial microbial mat (Baumgartner et al. 2006).

Girvanella-cortex oncoids

Description These oncoids ranges in size from 1 to 1.5 mm in diameter, with uneven, irregular, and nonsmooth cortices (Fig. 4a–c). The cortices of the oncoids associated with preserved fossils of *Girvanella* with either core of bioclasts (trilobite and/or brachiopods) (Fig. 4a–a′) or microbial envelop/bacterial biofilm (Fig. 4b–c). Further, observation shows the various shapes of oncoids that linked with the typical structure of cortex such as ellipsoidal in shape with rough and irregular laminations (Fig. 4a–a′), irregular shape with unevenly distribution of *Girvanella* in the cortex (Fig. 4b–b′), and rounded shape with an abundance of *Girvanella* in the outermost part of the cortex (Fig. 4c–c′). In addition, pyrite crystals are also observed in all these oncoids (Fig. 4a′, b′, c′). These oncoids are surrounded by sparite cement (Fig. 4a–c) that is relatively different from cementing material that observed in *Girvanella*-core oncoids (Fig. 3a–c).

Interpretation The *Girvanella* in the cortex of oncoid depicts the characteristics of laminated stromatolite (i.e., Riding 2011a, b). The oncoids with the core of bacterial biofilm (cyanobacteria and sulfate-reducing bacteria) show the similar features of the high-energy modern Bahamian coated grains that nucleus formed by the combination of cyanobacteria, sulfate-reducing bacteria, and diatoms (Brehm et al. 2003, 2006). These microorganisms excrete EPS in the microbial mat to form multiple biofilms (Decho 2010). Further EPS provides a substrate for precipitation of calcite in the Cambrian calcite sea (Stanley 2006; Dupraz et al. 2009; Mei et al. 2019c, 2020a, b). The oncoids with cores of bioclasts also depict the relatively high-energy setting of these deposits (Hanken et al. 2015; Riaz 2019). Moreover, the cementing material of these oncoids indicates the relatively low-energy setting as compared with the *Girvanella*-core oncoids that flourished in relatively high-energy setting above the normal wave base (Wang and Xiao 2018; Riaz 2019; Xiao et al. 2020a, b).

Girvanella-full oncoids

Description The petrographic observation shows the same composition from center to outermost cortices of the oncoids that mostly range in size from 1.5 to 2 mm in diameter (Fig. 5a–c). These oncoids are associated in variable shape, i.e., elliptical (Fig. 5a–a′), sub-angular (Fig. 5b–b′), and asymmetric (Fig. 5c–c′) that show the abundance of *Girvanella* in their

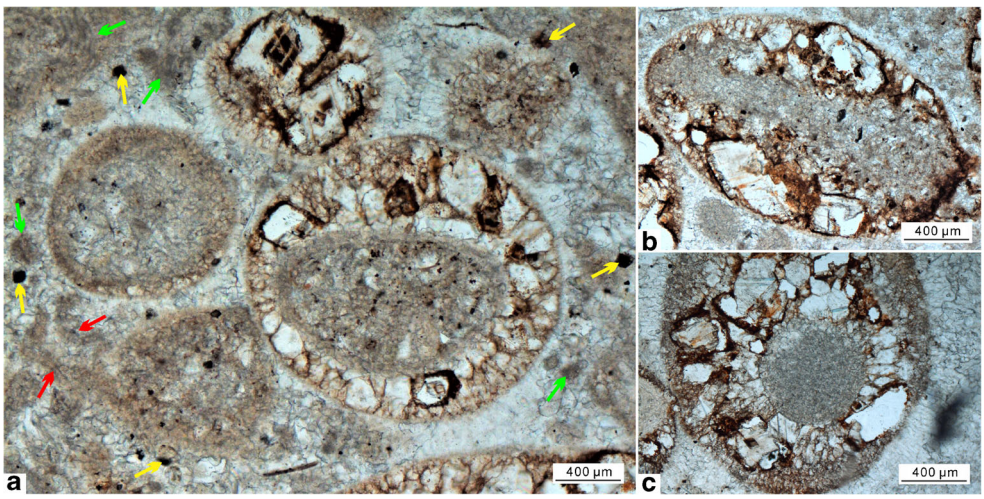

Fig. 3 Photomicrographs depict the Cambrian Miaolingian *Girvanella*-core oncoids in the NCP. **a** Oncoids showing rounded shapes that are associated with *Girvanella* in the core and crystals of dolomite in the cortex. The yellow arrows show the pyrite crystals. Red and green arrows indicate the bioclasts and patches of micrite, respectively. **b** Elliptical to the spheroidal shape of oncoids having an elliptical arrangement of *Girvanella* in the core. **c** Rounded shape of oncoid is due to the rounded shape of *Girvanella* core

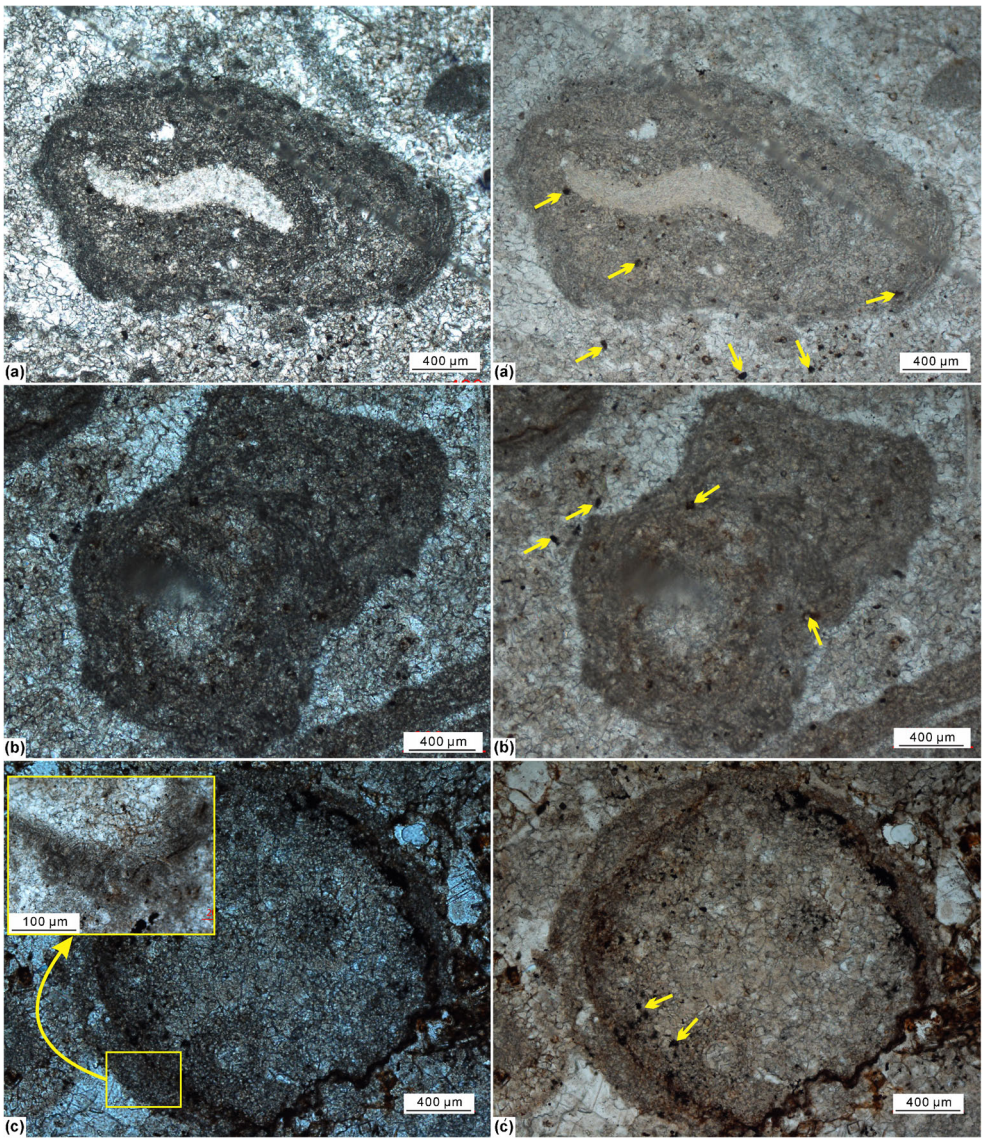

Fig. 4 Photomicrographs showing *Girvanella*-cortex oncoids surrounded by sparite cement. **a** An ellipsoidal oncoid with a core of trilobite/brachiopods/other bioclasts and a clotted cortex. **a′** Under cross-polarized light depicts the pyrite grains. **b** Irregular oncoid with a clotted and roughly laminated texture, comprised *Girvanella* fossils. **b′** Under cross-polarized light showing the irregular-shaped oncoids and pyrite grains. **c** Rounded oncoid grain, having roughly laminated cortices, with laminae thick upward and thin downward. **c′** Under cross-polarized light portray pyrite crystals.

cores and cortices (Fig. 5a–c). Further observations reveal the pyrite crystals in these oncoids (Fig. 5a′, b′). These oncoids are surrounded by sparite cement (Fig. 5a–c) similar to the cement observed in *Girvanella*-cortex oncoids (Fig. 4a–c).

Interpretation These oncoids are associated with the cortex of variable shape indicate the high-energy turbulence condition (i.e., Chow and James 1987; Heller et al. 1990). Further core and cortex predominantly comprise *Girvanella* fossils that indicate the involvement of filamentous cyanobacteria in the formation of Cambrian oncoids (i.e., Elliott 1975; Rees et al. 1989; Riding 1991; Mei et al. 2019a, b). Furthermore, pyrite crystals indicate a close connection with the sulfate reduction and may show the complex microbial precipitation inside the microbial mat during the formation of the oncoids (e.g., Dupraz et al. 2009; Riding 2011b). The cementing material of these oncoids is similar to *Girvanella*-cortex oncoids that indicate a relatively low-energy setting for their formation (Riaz 2019).

Geochemistry of oncoids

Trace elements

Table 1 lists the contents of the trace elements of the studied oncoids samples. Within the large ion lithophile elements (LILEs), Ba and Rb represent depletion (Table 1). In comparison, Rb is extremely depleted in studied oncoids of the NCP. Among LILEs, the Sr concentration within the oncoids is relatively higher (Table 1). In the case of Pb concentration, most of the oncoid samples reveal slight enrichment (Table 1). Among the ferromagnesian trace elements, Ni and Co indicate concentrations of 7.2–9.3 ppm and 0.74–1.91 ppm while Cr and V show contents of 1.2–2.4 ppm and 2.7–3.7 ppm respectively (Table 1). Within all of the high field strength elements (HFSEs) (Nb, Hf, Zr, Y, Th, and U), Nb, as well as Hf, is extremely depleted (Table 1).

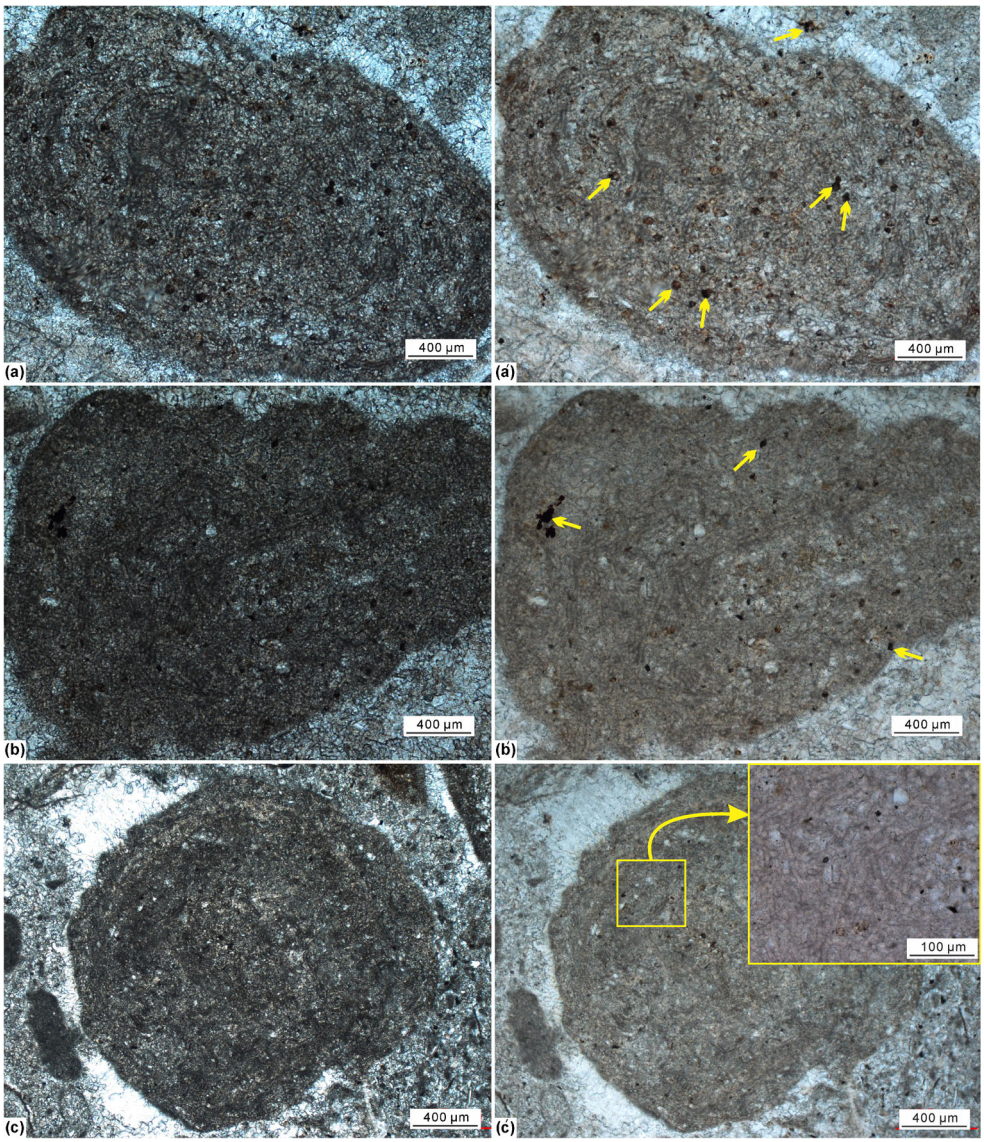

Fig. 5 Photomicrographs show *Girvanella*-full oncoids. **a–c** *Girvanella* growth in all stages of oncoids development. **a** Elliptical shape of oncoid without a nucleus is surrounded by sparite cement. **a′** Under cross-polarized light showing the pyrite crystals. **b** Sub-angular shape of oncoid associated with the same composition from center to outermost cortex. **b′** Under cross-polarized light filamentous *Girvanella* along with pyrite minerals. **c** Asymmetric shape of oncoid without a nucleus. **c′** Under cross-polarized light same feature observed and close view of *Girvanella* also shown

The studied oncoids indicate lower values of Mo/U ratios (1.10–2.46; average 1.76; Table 1). Most of the V/Cr ratios of oncoids are < 2, and V/(V + Ni) ratios vary from 0.24 to 0.33. Moreover, the variation of Sr/Cu between 42 and 54 and Sr/Ba (35–79) is presented in Table 1.

REEs

Table 1 presents the rare earth element contents (REEs) of the studied oncoids. On NASC-normalized REE pattern, these oncoids are observed with slightly weak negative Eu anomalies and indicates the weak enrichment of LREEs (Fig. 6). The Eu/Eu* ratios reveal a range of 0.34–1.03 (Table 1). Meanwhile, the variation of Ce/Ce* ratios in Cambrian oncoids ranges from 0.48 to 1.41 along with the absence of Ce anomaly (Table 1; Fig. 6). The oncoids are represented by higher Er/Nd and La/Yb ratios while most of the Gd/Gd* ratios of the Cambrian oncoids are < 1. The Y/Ho ratios of the Cambrian studied oncoids indicate a range of 30.17 and 42.08 (Table 1). The REE contents within the studied oncoids indicate a narrow range of 5.71 to 7.69 ppm with an average of 6.69 ppm (Table 1).

Discussion

Forming mechanism

Girvanella oncoids deposited in the Miaolingian strata of the NCP. These oncoids indicate high-energy depositional environment formed during FRST (forced regressive systems tract) of the third-order levels that represents a typical example of drowning unconformity (Schlager 1989, 1998, 1999). These oncoids are depicting dual characteristics, i.e.,

Table 1 Trace elements and rare earth element composition of Cambrian oncoids exposed in North China Platform (Data from Xiao et al. 2020)

Sample no.	Sc	V	Cr	Ni	Co	Zn	Cu	Rb	Sr	Y	Zr	Nb	Mo	Mo/U	Sb	
WH-XZ-1	1.124	3.214	1.692	8.231	1.911	8.547	2.926	0.171	124.022	0.798	6.961	0.403	0.512	2.42654	1.483	
WH-XZ-2	1.013	3.729	2.37	7.629	0.767	8.262	2.943	0.114	149.87	0.905	7.132	0.379	0.347	1.1051	1.355	
WH-XZ-3	0.892	2.923	2.413	8.654	1.032	9.301	2.868	0.152	131.073	0.957	7.126	0.652	0.498	2.09244	1.226	
DQ-ZX-1	0.925	3.241	1.699	8.618	1.228	9.469	2.447	0.139	132.135	0.922	6.712	0.142	0.493	1.95635	1.022	
DQ-ZX-2	0.844	3.164	1.722	8.146	1.453	8.897	2.571	0.14	131.674	1.039	6.303	0.089	0.409	2.05528	0.947	
DQ-ZX-3	0.782	2.776	1.214	7.88	1.393	7.324	2.415	0.143	132.383	1.104	6.57	0.162	0.389	1.61411	1.119	
XWD-XZ-1	0.873	3.215	1.417	7.282	1.13	8.225	2.523	0.151	123.01	0.984	4.948	0.556	0.431	1.42715	0.438	
XWD-XZ-2	0.921	2.872	1.524	7.648	0.889	9.374	2.631	0.143	121.101	0.831	5.122	0.579	0.318	1.2278	0.526	
XWD-XZ-3	0.782	2.964	1.736	8.125	0.925	7.209	2.422	0.168	128.645	0.935	5.251	0.404	0.425	1.17729	0.371	
SDG-ZX-1	0.926	3.422	2.375	9.361	0.747	9.062	2.492	0.117	113.002	1.01	4.036	0.075	0.385	1.90594	0.175	
SDG-ZX-2	0.771	2.941	2.141	9.243	1.028	8.452	2.545	0.122	120.801	1.142	4.425	0.105	0.479	2.46907	0.214	
SDG-ZX-3	0.917	3.218	2.288	8.736	0.857	8.209	2.381	0.105	117.925	0.831	4.001	0.069	0.392	1.66102	0.238	
Sample no.	**Ba**	**La**	**Ce**	**Pr**	**Nd**	**Sm**	**Eu**	**Gd**	**Tb**	**Dy**	**Ho**	**Er**	**Tm**	**Yb**	**Lu**	**Hf**
WH-XZ-1	1.637	1.038	1.906	0.437	0.513	0.428	0.062	0.301	0.03	0.071	0.026	0.063	0.016	0.127	0.0121	0.054
WH-XZ-2	1.902	1.025	1.825	0.328	0.591	0.344	0.049	0.29	0.044	0.094	0.03	0.051	0.019	0.124	0.013	0.041
WH-XZ-3	1.643	1.007	2.031	0.384	0.369	0.274	0.026	0.192	0.011	0.088	0.031	0.036	0.013	0.118	0.018	0.057
DQ-ZX-1	2.329	0.926	2.267	0.221	0.276	0.392	0.041	0.224	0.056	0.076	0.029	0.049	0.018	0.078	0.022	0.045
DQ-ZX-2	2.415	0.985	2.338	0.189	0.425	0.301	0.027	0.313	0.019	0.064	0.032	0.048	0.012	0.065	0.015	0.042
DQ-ZX-3	2.331	1.013	2.825	0.246	0.385	0.356	0.034	0.294	0.025	0.055	0.033	0.054	0.017	0.082	0.014	0.065
XWD-XZ-1	1.997	0.909	1.792	0.346	0.328	0.217	0.038	0.33	0.053	0.063	0.029	0.062	0.018	0.133	0.019	0.059
XWD-XZ-2	2.14	0.973	1.604	0.391	0.264	0.192	0.059	0.295	0.032	0.056	0.023	0.053	0.014	0.142	0.018	0.042
XWD-XZ-3	2.329	0.902	1.737	0.286	0.343	0.208	0.071	0.248	0.048	0.049	0.026	0.064	0.012	0.11	0.017	0.058
SDG-ZX-1	2.842	0.964	1.342	0.192	0.205	0.264	0.039	0.32	0.021	0.044	0.024	0.042	0.023	0.081	0.024	0.031
SDG-ZX-2	3.431	0.982	1.479	0.207	0.232	0.298	0.037	0.286	0.039	0.052	0.028	0.049	0.011	0.073	0.018	0.033
SDG-ZX-3	2.925	0.951	1.53	0.233	0.218	0.285	0.051	0.341	0.051	0.047	0.023	0.051	0.011	0.095	0.013	0.029
Sample no.	**Ta**	**Pb**	**Th**	**U**	**V/Sc**	**V/Cr**	**Sr/Ba**	**Sr/Cu**	**V/V+ Ni**	**Th/U**	**Cu/Zn**					
WH-XZ-1	0.023	1.981	0.394	0.211	2.86	1.9	75.76	42.39	0.28	1.87	0.34					
WH-XZ-2	0.037	1.842	0.458	0.314	3.68	1.57	78.8	50.92	0.33	1.46	0.36					
WH-XZ-3	0.018	1.983	0.411	0.238	3.28	1.21	79.78	45.7	0.25	1.73	0.31					
DQ-ZX-1	0.009	1.104	0.392	0.252	3.5	1.91	56.73	53.99	0.27	1.56	0.26					
DQ-ZX-2	0.012	1.302	0.385	0.199	3.75	1.84	54.52	51.21	0.28	1.93	0.29					
DQ-ZX-3	0.025	1.228	0.407	0.241	3.55	2.29	56.79	54.82	0.26	1.69	0.33					
XWD-XZ-1	0.017	1.617	0.548	0.302	3.68	2.27	61.6	48.76	0.31	1.81	0.31					
XWD-XZ-2	0.029	1.536	0.419	0.259	3.12	1.88	56.59	46.03	0.27	1.62	0.28					
XWD-XZ-3	0.016	1.429	0.371	0.361	3.79	1.71	55.24	53.12	0.27	1.03	0.34					
SDG-ZX-1	0.013	1.632	0.397	0.202	3.7	1.44	39.76	45.35	0.27	1.97	0.27					
SDG-ZX-2	0.011	1.307	0.374	0.194	3.81	1.37	35.21	47.47	0.24	1.93	0.3					
SDG-ZX-3	0.012	1.453	0.382	0.236	3.51	1.41	40.32	49.53	0.27	1.62	0.29					
Sample no.	**REE**	**Er/Nd**	**Y/Ho**	**Ce/Ce***	**Pr/Pr***	**Eu/Eu***	**Gd/Gd***	**Nd_N**	**Yb_N**	**$(Nd/Yb)_N$**	**La/Yb**					
WH-XZ-1	7.69	0.12	30.7	0.51	0.23	0.6	0.78	0.86	0.61	1.40984	8.17					
WH-XZ-2	7.52	0.09	30.17	0.64	0.17	0.57	0.71	0.98	0.59	1.66102	8.26					
WH-XZ-3	7.31	0.1	30.87	0.61	0.22	0.39	1.25	0.62	0.56	1.10714	8.53					
DQ-ZX-1	6.48	0.17	31.79	1.17	0.13	0.45	0.51	0.46	0.37	1.24324	11.87					
DQ-ZX-2	6.77	0.11	32.47	1.41	0.09	0.34	1.57	0.71	0.31	2.29032	15.15					
DQ-ZX-3	7.39	0.14	33.45	1.32	0.11	0.38	1.15	0.64	0.39	1.64103	12.35					
XWD-XZ-1	6.88	0.19	33.93	0.6	0.22	0.59	0.79	0.55	0.64	0.85938	6.83					
XWD-XZ-2	6.4	0.2	36.13	0.48	0.29	1.03	0.77	0.44	0.68	0.64706	6.85					
XWD-XZ-3	6.36	0.19	35.96	0.7	0.18	1.24	0.48	0.57	0.53	1.07547	8.20					
SDG-ZX-1	5.86	0.2	42.08	0.8	0.18	0.54	1.26	0.34	0.39	0.87179	11.90					
SDG-ZX-2	5.71	0.21	40.79	0.82	0.17	0.48	0.84	0.39	0.35	1.11429	13.45					
SDG-ZX-3	6.01	0.23	36.13	0.75	0.19	0.65	0.75	0.36	0.45	0.8	10.01					

WH= Wuhai Section-Inner Mongolia Province

DQ= Diaoquan Section-Shanxi Province

XWD= Xiaweidian Section-Beijing

SDG= Sandaogou Section-Liaoning Province

XZ= Xuzhuang Formation

ZX= Zhangxia Formation

laminated stromatolites and mobile coated grains that represent a spectacular sedimentary phenomenon (Bosak et al. 2013; Pederson et al. 2015; Peters et al. 2017). The abundantly preserved *Girvanella* in these oncoids shows its involvement at different growth stages that significantly alter the microstructure and consequently, different types of *Girvanella*

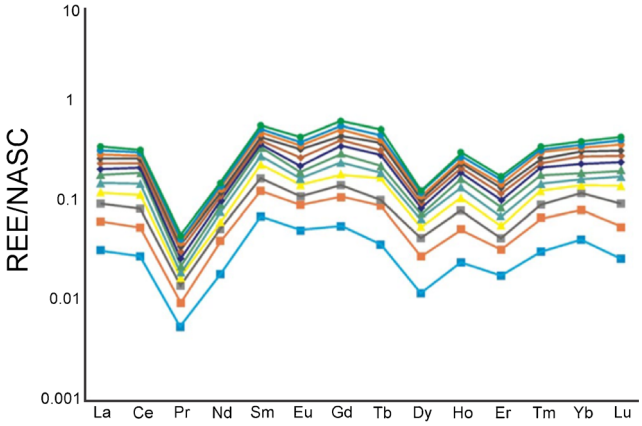

Fig. 6 NASC-normalized REE patterns of oncoids indicating slightly weak negative Eu anomalies and weak enrichment of LREEs

oncoids are developed (Fig. 7). In *Girvanella*-core oncoids, *Girvanella* along with few heterotrophic organisms make a dark micrite in the center of the oncoids (Figs. 3a–c and 7). These microorganisms particularly cyanobacteria excrete gel-like material called extracellular polymeric substance (EPS) that provides the substrate for endorsing precipitation of $CaCO_3$ (Dupraz et al. 2009; Bosak 2011; Decho and Gutierrez 2017). In the *Girvanella*-cortex oncoids, *Girvanella* filaments were involved in the development of the cortices. Consequent calcification caused the development of *Girvanella*-rich laminae, which served as textural elements of these oncoids. Similarly, *Girvanella*-full oncoids experienced all stages of *Girvanella* growth as compared with the first two forms of *Girvanella* oncoids (Fig. 7). The presence of *Girvanella* in all stages of oncoids demonstrates credible confirmation regarding the contribution of *Girvanella* in the development of these carbonate grains. Furthermore, petrographic observations clarify that *Girvanella*-core oncoids flourished under high-energy conditions above the normal wave base, whereas *Girvanella*-cortex and *Girvanella*-full oncoids deposited in both high and relatively low-energy settings above and below the normal wave base.

The cores and cortices of these oncoids are composed of *Girvanella* and sulfate-reducing bacteria (Figs. 3, 4, 5, and 7) that are a possible demonstration of the microbial origin of the Cambrian oncoids of the NCP. These *Girvanella* fossils are equivalent to either the modern *Plectonema* (Riding 1991) or the modern *Tychonema* (De los Ríos et al. 2015). The evenly outlined walls of the *Girvanella* fossil can be interpreted as a

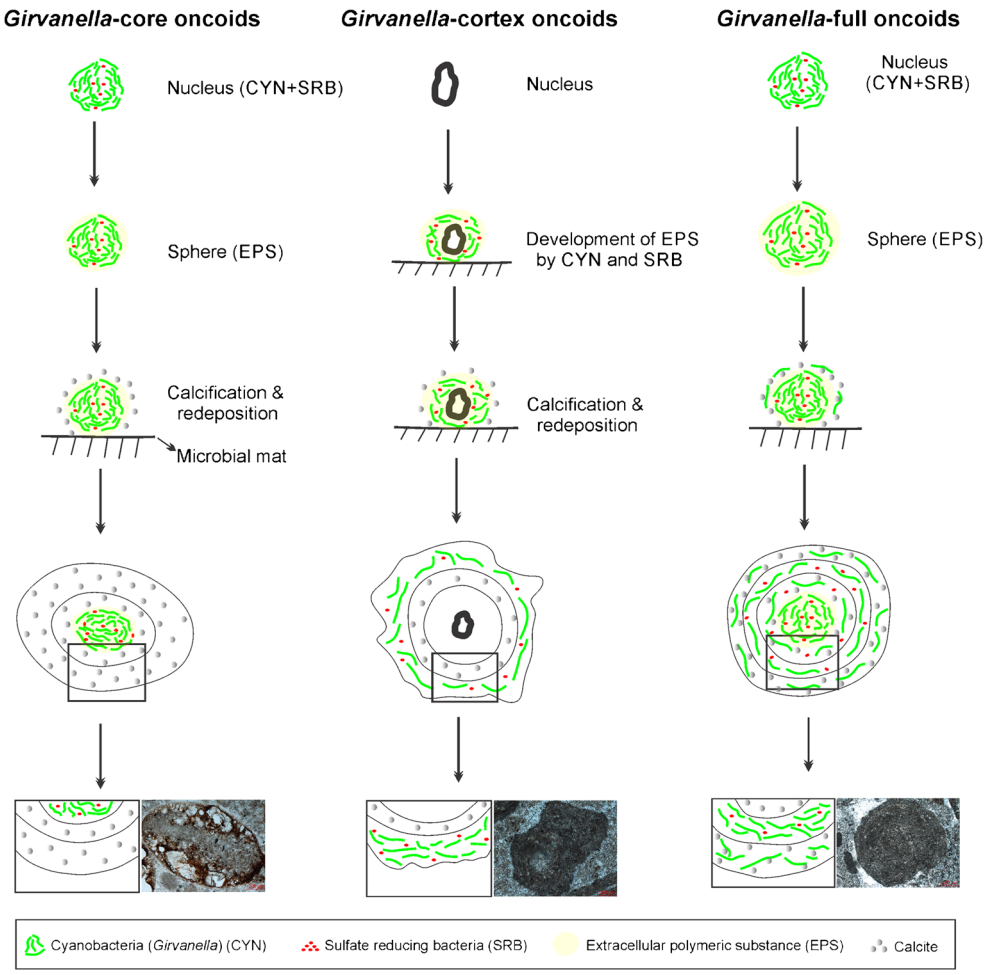

Fig. 7 Schematic illustrations of the Cambrian oncoids in the NCP. The sketch describes the involvement of *Girvanella* in different modes of oncoids development.

residue of *in vivo* calcification that represents an ecophysiological mechanism, which is genetically related to the atmospheric carbon dioxide concentration mechanisms (CCMs; Riding 2000; Kah and Riding 2007). Moreover, the *in vivo* calcification may coordinate with calcification of EPSs containing extracellular sunscreen scytonemin (Soule et al. 2009; Mei et al. 2020a), which is different from the calcification of common EPSs forming microbial mats. The interior parts of filaments are filled by microspars that may be the residues of cyanobacterial cells. Further, the filamentous fossils in the cores (Fig. 3) and cortices of oncoids (Figs. 4 and 5) strongly reflect the sophisticated calcification of photosynthetic biofilms that occurred after the *in vivo* calcification of cyanobacterial sheaths (Riding 2000; Reitner 2011a, b). These credible pieces of evidence provide certain clues of the microbial origin of Cambrian oncoids of the NCP. However, it is difficult to reach certain conclusions whether *Girvanella* fossils are directly involved in the formation of oncoids or not; nevertheless, these fossils provide certain evidences for the microbial origin of oncoids.

Furthermore, the presence of pyrite crystal in the Cambrian oncoids indicates microbial precipitation which is related to sulfate reduction (Riding 2000; Baumgartner et al. 2006). Moreover, pyrite crystals describe two important factors, i.e., alkalinity engine (Kempe and Kazmierczak 1994; Gallagher et al. 2012) and EPS (Tourney and Ngwenya 2014; Decho and Gutierrez 2017), which actively participate in carbonate precipitation in the cortex and core of these oncoids. In other words, cyanobacteria (*Girvanella*) abundantly and successively excrete a mess of EPSs to form biofilm in the microbial mat, and its degradation via heterotrophic organisms like sulfate-reducing bacteria caused the precipitation. The exact mechanism of precipitation in microbial mats dominated by *Girvanella* is still an important subject that needs to be investigated in the future.

Geochemical characteristics and source of REEs in Cambrian oncoids

Rare earth elements (REEs) in carbonate bodies are mainly inherited from ancient seawater. But, in several cases, the concentrations of REEs in ancient carbonates such as oncoids were also affected by detrital involvement as well as diagenesis. Thus, REEs of oncoids can be significant to reveal the participation of terrigenous input in addition to diagenetic influence. The rare earth elements (REEs) ratios such as Eu/Eu* can be valuable to infer the involvement of terrigenous material during the carbonates formation. The Eu/Eu* ratios of the Cambrian oncoid samples indicate a range of 0.34–1.03 (Table 1). In general, the slightly positive Eu anomalies in REE patterns which are rare in seawater possibly caused by the diagenetic variations in the carbonates (Abiding and Calagari 2015) and enhanced through processes of hydrothermal activities (Madhavaraju and Lee 2009). On the contrary, the slightly negative anomalies of Eu are indicative of the terrigenous input in carbonate samples (Dai et al. 2016). The slightly negative Eu anomalies in the studied oncoids suggest that these oncoids have been subjected to terrigenous participation during their formation (Fig. 6). Therefore, based on these findings, we propose that the slightly negative Eu anomalies in oncoids are indicative of terrigenous involvement.

Several research works have been conducted on the variations of Ce in the marine settings for defining paleoenvironments (e.g., Nath et al. 1997). Also, it is documented that the scarcity of Ce in oceanic water is due to redox variations of Ce (Elderfield 1988). The variation of Ce/Ce* ratios in Cambrian oncoids ranges between 0.48 and 1.41 (Table 1). Both Ce contents and the lack of Ce anomaly in studied oncoids can be governed by lithological input, and diagenesis may impart an important character in the incorporation of REEs (particularly Ce). According to Armstrong-Altrin et al. (2001), the diagenesis can indicate a worthy character in removing Ce anomaly in the samples of oncoids. Considering these views, it is suggested that the absence of Ce anomaly in Cambrian oncoids can be attributed to diagenetic activities. Further, the impact of diagenetic conditions is most likely defined by Er/Nd ratios (Abiding and Calagari 2015). Their higher ratios in carbonates show the seawater signature conserved by the sediments. It is widely reported that the ratio (Er/Nd) is nearly 0.27 in normal seawater (De Baar et al. 1988). Both diagenetic processes and terrigenous materials can be responsible for discretional amounts of Nd comparative to Er and may decrease the Er/Nd values to < 0.1 (Abiding and Calagari 2015). However, these ratios in the oncoids vary between 0.09 and 0.23. Fairly higher values of Er/Nd (Table 1) point out that the impact of terrigenous materials and diagenetic activities was insignificant. Relatively greater values of Er/Nd in oncoids of the NCP indicate seawater signature conserved by the marine sediments.

The Gd/Gd* ratios of the carbonates of modern shallow seawater range from 1.05 to 1.30, as indicated by De Baar et al. (1985). However, most of the Gd/Gd* ratios of the Cambrian oncoids are < 1 (Table 1), suggesting the influence of diagenetic processes on the oncoids of the NCP. The super chondritic Y/Ho ratios of the studied oncoids are less than the values of seawater (~ 44–74) as defined by Bau (1996). Relatively lesser values of oncoids in comparison to sea water suggest the impact of diagenetic activities on the carbonates of the studied area. Meanwhile, the higher La/Yb values (Table 1) of oncoids (6.8–15.1) suggest the involvement of limited detrital material during the genesis of Cambrian oncoids (Sholkovitz 1990; Condie 1991). Considering these views, it can be concluded that the oncoids of the NCP have been influenced by diagenetic activities and limited terrigenous input during their formation.

The REE patterns in carbonates are frequently significant to typify source rocks (Tobia 2018). NASC-normalized REEs values of the studied oncoids are mostly depleted and this points out the contribution of detrital material within the Cambrian oncoids (Fig. 6; Sen and Mishra 2015). The studied samples reflect a narrow range of discrepancy in ΣREE contents (5.71 to 7.69, average 6.69; Table 1). These narrow ranges in contents of ΣREE are also a consequence of variation in detrital materials within the Cambrian oncoids (Chen et al. 2014).

The $(Nd/Yb)_N$ ratios of the oncoids differ from 0.64 to 2.29 (Table 1) and are not comparable to the seawater-like REE patterns. Therefore, oncoids with higher $(Nd/Yb)_N$ ratios confirm that the source of these REE ratios is from terrigenous input within the Cambrian oncoids. Meanwhile, it is also widely accepted that higher ratios of Er/Nd indicate that they are sourced and preserved by marine carbonates (De Baar et al. 1988). On the contrary, the ratios of Er/Nd having values less than 0.1 are suggestive of terrigenous input and diagenetic activities within the oncoids (Tobia 2018). Therefore, the ratios Er/Nd, $(Nd/Yb)_N$, La/Yb, and depletion and variation of REEs point out the occurrence of a detrital fraction which is the most credible source of REEs within the oncoids. The Er/Nd ratios of the oncoids are within the range of 0.09 to 0.23 (Table 1), indicating that these higher rare earth elemental ratios are sourced and preserved by marine carbonates (De Baar et al. 1988).

Implications on paleoenvironments of Cambrian oncoids

Several researches have reported that the positive Eu anomalies are owing to hydrothermal activities (Armstrong-Altrin et al. 2003) or because of diagenetic alteration (Tobia 2018). The studied oncoids are flourished in shallow carbonate platform (Xiao et al. 2020a); thus, local enhancement of feldspar as well as diagenetic variations can produce positive Eu anomaly. However, on the REE pattern, the observed oncoids of the NCP show weak negative Eu anomalies (Fig. 6). These observed negative anomalies point out the preservation of the original marine water signatures within the oncoids.

Y/Ho ratio is reflected as one of the consistent tool for the marine environment (Xiao et al. 2020a). In modern marine settings, this ratio differs between 40 and 90 (Bau 1999). The Y/Ho ratios of the Cambrian studied oncoids indicate a range of 30.17 and 42.08 (Table 1) with an average value of 34.53. This implies that the oncoids have thrived in a marine setting; however owing to the detrital input or because of the diagenesis, the average Y/Ho ratio of the oncoids is declined (Tobia 2018). Further, this ratio is analogous to other Mesoproterozoic carbonates such as Rohtas carbonates (Banerjee and Jeevankumar 2007). The observed larger variations in the Y/Ho ratios of the oncoids exhibit that the studied oncoids are contaminated by the impact of detrital materials. The lower values of the Y/Ho ratio such as 30.17 to 33.93 in the studied oncoids also propose freshwater participation from the rivers in the seawater during precipitation of these Cambrian oncoids.

Modern studies report that the geochemical ratios such as Mo/U are significant pointers of redox conditions of carbonates (McManus et al. 2006). Therefore, these conditions of oncoids can be rebuilt by trace elemental ratios present in the studied oncoids. Algeo and Tribovillard (2009) confirmed that Mo/U ratios higher than 7.9 are considered as a pointer of anoxic/sulfidic conditions and can provide significant information by studying sediments from modern marine settings. However, the studied oncoids indicate lower values of Mo/U ratios (1.10–2.46; average 1.76; Table 1). Lower values of Mo/U ratios of studied oncoids suggest that oncoids thrived in oxic environments.

Several researches reported the application of Ce anomaly in the marine environments for highlighting the paleo conditions (Hua et al. 2013; Khelen et al. 2017). To decide the redox condition, Ce anomalies are consistent and more reliable since Ce valences and solubility differ in redox condition. Under the oxidized environment, a negative or lack of Ce anomaly promotes (Hua et al. 2013). However, under anoxic condition, positive Ce anomaly results. In this study, the oncoids are displaying a deficiency of Ce anomaly (Fig. 6), which suggests deposition of oncoids under the oxic environment.

In addition, V/(V + Ni) and V/Cr are important to define the paleoenvironmental conditions of carbonates (Xiao et al. 2020a). Low V/Cr ratio (< 2) is suggestive of oxic conditions, and V/(V + Ni) < 0.6 also represents the oxidizing condition (Rimmer 2004; Xiao et al. 2020a). Similarly, most of the V/Cr ratios of oncoids are < 2, and V/(V + Ni) ratios vary from 0.24 to 0.33 (Table 1), suggesting the flourishment of Cambrian oncoids under oxic conditions.

The Sr/Cu and Sr/Ba ratios are measured as significant proxies to delineate paleoclimatic conditions of carbonates (Fouke et al. 2005). It is widely reported that the range of Sr/Cu (1.3 to 5.0) shows humid climate, whereas higher than 5.0 displays arid climate (Ni et al. 2010). The oncoids of this study represent a variation of Sr/Cu between 42 and 54 (Table 1), signifying arid climatic environments. Moreover, if the Sr/Ba value is < 1, it is representative of terrestrial condition; nonetheless, greater than 1 value of Sr/Ba is suggestive of marine condition (Tripati et al. 2009). The studied oncoids reveal the variation of Sr/Ba (35–79), signifying classic marine conditions.

Considering the above discussion regarding paleoenvironmental analyses of Cambrian oncoids, it can be concluded that the oncoids of the North China Platform (NCP) flourished under oxic, arid, and classic marine conditions.

Conclusions

1) *Girvanella* oncoids of the North China Platform (NCP) were distinguished into *Girvanella*-core, *Girvanella*-cortex, and *Girvanella*-full oncoids based on the morphology of the cortices. *Girvanella*-core oncoids indicate both high and relatively low-energy depositional settings based on the cementing material and the thickness of the cortex, while *Girvanella*-cortex oncoids and *Girvanella*-full oncoids are formed under relatively low-energy settings. These oncoids are associated with EPSs, which form a number of biofilms in a relatively thick microbial mat dominated by cyanobacteria, where they grow and roll over it. Moreover, abundantly preserved filamentous fossils, i.e., *Girvanella* in the cortex and nuclei of oncoids, strongly suggest the independent growth of these oncoids over microbial mats. The presence of pyrite grains and dolomite crystals in these oncoids also clarifies the calcification and decomposition of EPSs in cyanobacteria-dominated microbial mats.
2) The slightly negative Eu anomalies, higher La/Yb values, and the observed larger Y/Ho variations in the Cambrian oncoids of NCP suggest that these oncoids have been subjected to terrigenous participation during their formation. Considering the absence of Ce anomaly, Gd/Gd* ratios (< 1) and lesser values of Y/Ho, it can be concluded that the oncoids of the NCP have been influenced by diagenetic activities. Relatively greater values of Er/Nd suggest seawater signature preserved by the marine sediments. In addition, observed weak negative Eu anomalies within the oncoids point out the retention of the original marine water characteristics while lower values of the Y/Ho propose freshwater participation from the rivers in the seawater during precipitation of oncoids.
3) Based on the ratios Er/Nd, $(Nd/Yb)_N$, La/Yb, and depletion and variation of REEs, it can be confirmed that the source of these REEs within the oncoids is mainly from terrigenous input, which is the most credible source of REEs. However, the higher Er/Nd ratios are sourced and preserved by marine carbonates.
4) Lower values of Mo/U, V/Cr, and V/(V + Ni) ratios and deficiency of Ce anomaly in the studied oncoids suggest that these oncoids were flourished under oxic environments. These oncoids represent a variation of Sr/Cu between 42 and 54 and Sr/Ba (35–79), suggesting their development under arid climatic conditions and classic marine settings.

Acknowledgments We gratefully acknowledge Professor Mei Mingxiang (China University of Geosciences Beijing), who provided us financial support from the National Natural Science Foundation of China (Grant No. 41472090), and guided us in the fieldwork. We are thankful to Editor Dr. Santanu Banerjee and the anonymous reviewers, for their fruitful suggestions to improve the quality of the paper.

Compliance with ethical standards

Conflict of interest The authors declare that there is no conflict of interest.

References

Abiding A, Calagari AA (2015) Rare earth element geochemistry of the Upper Permian limestone: the Kanigorgeh mining district, NW Iran. Turk J Earth Sci 24:365–382

Algeo TJ, Tribovillard N (2009) Environmental analysis of paleoceanographic systems based on molybdenum-uranium covariation. Chem Geol 268(3-4):211–225

Armstrong-Altrin SJ, Ramasamy S, Makhnach A (2001) Stable isotopes geochemistry and evidences for meteoric diagenesis in Kudankulam Formation, Tamil Nadu. J Geol Soc India 57:39–48

Armstrong-Altrin JS, Verma SP, Madhavaraju J, Lee YI, Ramasamy S (2003) Geochemistry of Upper Miocene Kudankulam Limestones, southern India. Int Geol Rev 45:16–26

Banerjee S, Jeevankumar S (2007) Facies and depositional sequence of the Mesoproterozoic Rohtas Limestone: Eastern Son valley, Vindhyan basin. J Asian Earth Sci 30(1):82–92

Bau M (1996) Controls on the fractionation of isovalent trace elements in magmatic and aqueous systems: evidence from Y/Ho, Zr/Hf, and lanthanide tetrad effect. Contrib Mineral Petrol 123:323–333

Bau M (1999) Scavenging of dissolved yttrium and rare earths by precipitating Fe oxyhydroxide: experimental evidence for Ce oxidation, Yho fractionation, and lanthanide tetrad effect. Geochim Cosmochim Acta 63:67–77

Baumgartner LK, Reid RP, Dupraz C, Decho AW, Buckley DH, Spear JR, Przekop KM, Visscher PT (2006) Sulfate reducing bacteria in microbial mats: Changing paradigms, new discoveries. Sediment Geol 185:131–145

Bosak T (2011) Calcite precipitation microbially induced. In: Reitner J, Thiel V (eds) Encyclopedia of geobiology. Springer, Berlin Heidelberg, New York, pp 223–226

Bosak T, Knoll AH, Petroff AP (2013) The meaning of stromatolites. Annu Rev Earth Planet Sci 41:21–44

Brehm U, Krumbein WE, Palinska KA (2003) Microbial spheres: a novel cyanobacterial-diatom symbiosis. Naturwiss 90:136–140

Brehm U, Krumbein WE, Palinska KA (2006) Biomicrospheres generate ooids in the laboratory. Geomicrobiol J 23:545–550

Brett CE, Mclaughlin PI, Histon K, Schindler E, Ferretti A (2012) Time-specific aspects of facies: state of the art, examples, and possible causes. Palaeogeogr Palaeocl 367–368:6–18

Brigaud B, Durlet C, Deconinck JF, Vincent B, Pucéat E, Thierry J, Trouiller A (2009) Facies and climate/environmental changes recorded on a carbonate ramp: A sedimentological and geochemical approach on Middle Jurassic carbonates (Paris Basin, France). Sediment Geol 222(3):181–206

Chen S, Gui H, Sun L (2014) Geochemical characteristics of REE in the late neo-proterozoic limestone from the northern Anhui Province, China. Chin J Geochem 33:187–193

Chow N, James NP (1987) Facies-specific, calcitic and bimineralic ooids from Middle and Upper Cambrian platform carbonates, western Newfoundland, Canada. J Sediment Petrol 57:907–921

Condie KC (1991) Another look at rare earth elements in shales. Geochim Cosmochim Acta 55:2527–2531

Dahanayake K (1977) Classification of oncoids from the Upper Jurassic carbonates of the French Jura. Sediment Geol 18:337–353

Dai S, Graham IT, Ward CR (2016) A review of anomalous rare earth elements and yttrium in coal. Int J Coal Geol 159:82–95

De Baar HJW, Bacon MP, Brewer PG (1985) Rare earth elements in the Pacific and Atlantic oceans. Geochim Cosmochim Acta 49:1943–1959

De Baar HJW, German CR, Elderfield H, Van Gaans P (1988) Rare earth element distributions in anoxic waters of the Cariaco Trench. Geochim Cosmochim Acta 52:1203–1219

De los Ríos A, Ascaso C, Wierzchos J, Vincent WF, Quesada A (2015) Microstructure and cyanobacterial composition of microbial mats from the High Arctic. Biodivers Conserv 24:841–863

Decho AW (2010) Overview of biopolymer-induced mineralization: what goes on in biofilms? Ecol Eng 36:137–144

Decho AW, Gutierrez T (2017) Microbial extracellular polymeric substances (EPSs) in ocean systems. Front Microbiol 8:1–28

Diaz MR, Eberli GP (2019) Decoding the mechanism of formation in marine ooids: a review. Earth Sci Rev 190:536–556

Duguid SM, Kyser TK, James NP, Rankey EC (2010) Microbes and ooids. J Sediment Res 80(3):236–251

Dupraz C, Reid RP, Braissant O, Decho AW, Norman RS, Visscher PT (2009) Processes of carbonate precipitation in modern microbial mats. Earth-Sci Rev 96:141–162

Elderfield H (1988) Tracer in the ocean – the oceanic chemistry of the rare-earth elements. Phil Trans R Soc A 325:105–126

Elliott GF (1975) Transported algae as indicators of different marine habitats in the English Middle Jurassic. Palaeontology 18:351–366

Flügel E (2004) Microfacies of carbonate rocks. Springer, Berlin Heidelberg New York, 976pp

Flügel E, Munnecke A (2010) Microfacies of carbonate rocks. Springer-Verlag, Berlin, pp 128–129

Fouke BW, Schlager W, Vandamme MG, Henderiks J, Van Hilten B (2005) Basin-to-platform chemostratigraphy and diagenesis of the Early Cretaceous Vercors Carbonate Platform, SE France. Sediment Geol 175(1–4):297–314

Gallagher KL, Kading TJ, Braissant O, Dupraz C, Visscher PT (2012) Inside the alkalinity engine: the role of electron donors in the organomineralization potential of sulfate-reducing bacteria. Geobiology 10:518–530

Guo Q, Jin ZK, Zhu X, Shi ST, Wang JJ, Wang JY, Li Y, Li S (2020) Characteristics and mechanism of dolomitization in the ooids of the Cambrian Zhangxia Formation, Xiaweidian, China. Carbonates Evaporites 35:7. https://doi.org/10.1007/s13146-019-00545-9

Han Z, Zhnag X, Chi N, Han M, Woo J, Lee HS, Chen J (2015) Cambrian oncoids and other microbial-related grains on the North China Platform. Carbonates Evaporites 30:373–386

Hanken NM, Bjorlykke K, Nielsen JK (2015) Carbonate Sediments. In: Bjorlykke K (ed) Petroleum geoscience: from sedimentary environments to rock physics. Springer-Verlag, Berlin, pp 151–216

Helland-Hansen W, Gjelberg JG (1994) Conceptual basis and variability in sequence stratigraphy: a different perspective. Sediment Geol 92: 31–52

Heller PL, Komar PD, Pevear DR (1980) Transport processes in ooid genesis. J Sediment Res 50:943–952

Jones B (1992) Void-filling deposits in karst terrains of isolated oceanic islands: a case study from Tertiary carbonates of the Cayman Islands. Sedimentology 39(5):857–876

Jones B (2011) Biogenicity of terrestrial oncoids formed in soil pockets, Cayman Brac, British West Indies. Sediment Geol 236(1):95–108

Jones B, Renaut RW (2010) Impact of seasonal changes on the formation and accumulation of soft siliceous sediments on the discharge apron of Geysir, Iceland. J Sediment Res 80(1):17–35

Kah LC, Riding R (2007) Mesoproterozoic carbon dioxide levels inferred from calcified cyanobacteria. Geology 35:799–802

Kempe S, Kazmierczak J (1994) The role of alkalinity in the evolution of ocean chemistry, organization of living systems, and biocalcification processes. Bull Inst Océanogr Monaco 13:61–117

Khelen AC, Manikyamba C, Ganguly S, Singh TD, Subramanyam KSV, Ahmad SM, Reddy MR (2017) Geochemical and stable isotope signatures of Proterozoic stromatolitic carbonates from the Vempalle and Tadpatri formations, Cuddapah Supergroup, India: implications on paleoenvironment and depositional conditions. Precambrian Res 298:365–384

Liu W, Zhang X (2012) *Girvanella*-coated grains from Cambrian oolitic limestone. Facies 58:779–787

Madhavaraju J, Lee YI (2009) Geochemistry of the Dalmiapuram Formation of the Uttatur Group (Early Cretaceous), Cauvery basin, southeastern India: implications on provenance and paleo-redox conditions. Rev Mex Cienc Geol 26:380–394

McManus J, Berelson WM, Severmann S, Poulson RL, Hammond DE, Klinkhammer GP, Holm C (2006) Molybdenum and uranium geochemistry in continental margin sediments: Paleoproxy potential. Geochim Cosmochim Acta 70(18):4643–4662

Mei MX (1996) Carbonate third-order cyclic sequence of the drowning-unconformity type: discussion on the condensation of carbonate platform. Sediment Facies Paleogeogr 16(6):24–33 (in Chinese with English abstract)

Mei MX (2010) Correlation of sequence boundaries according to discerning between normal and forced regressions: the first advance in sequence stratigraphy. J Palaeogeogr 12(5):549–564 (in Chinese with English abstract)

Mei MX (2011) Depositional trends and sequence-stratigraphic successions under the Cambrian second-order transgressive setting in the North China Platform: a case study of the Xiaweidian section in the western suburb of Beijing. Geol China 38(2):317–337 (in Chinese with English abstract)

Mei MX, Riaz M, Liu L, Meng QF (2019a) Oncoids built by photosynthetic biofilms: an example from the Series 2 of Cambrian at Fuzhouwan section in Liaodong Peninsula. J Palaeogeogr 21(1): 37–54 (in Chinese with English Abstract)

Mei MX, Riaz M, Meng QF, Liu L (2019b) Particular cap oncolitic grainstones of bank oolitic grainstones–an example from the Zhangxia Formation of the Cambrian Miaolingian at the Chafangzi Section in Fanshi County of Shanxi Province, North China. Geol Rev 65(4):839–856 (in Chinese with English Abstract)

Mei MX, Riaz M, Liu L, Meng QF (2019c) Leiolite bioherm dominated by cyanobacterial mats of the Furongian: an example from the Qijiayu section in Laiyuan County, Hebei Province. Geol Rev 65(5):1103–1122 (in Chinese with English Abstract)

Mei MX, Latif K, Mei CJ, Gao J, Meng QF (2020a) Thrombolitic clots dominated by filamentous cyanobacteria and crusts of radio-fibrous calcite in the Furongian Changshan Formation, North China, Sediment Geol 395. https://doi.org/10.1016/j.sedgeo.2019.105540,

Mei CJ, Riaz M, Long W, Latif K, Rui Z (2020b) Development of Middle Cambrian leiolitic bioherms dominated by calcified microbes: a case study of the Xinji Section (North China Platform). Mar Microplaentol 157:101858. https://doi.org/10.1016/j.marmicro.2020.101858

Meng X, Ge M, Tucker ME (1997) Sequence stratigraphy, sea-level changes and depositional systems in the Cambro-Ordovician of the North China carbonate platform. Sediment Geol 114:189–222

Myrow PM, Chen J, Snyder Z, Leslie S, Fike D, Fanning M, Yuan J, Tang P (2015) Depositional history, tectonics, and provenance of the Cambrian-Ordovician succession in the western margin of the North China Block. Geol Soc Am Bull 127:1174–1193

Nath BN, Bau M, Rao BR, Rao CM (1997) Trace and rare earth elemental variation in Arabian Sea sediments through a transect across the oxygen minimum zone. Geochim Cosmochim Acta 61:2375–2388

Ni T, Corcoran DL, Rach EA, Song S, Spana EP, Gao Y, Zhu J (2010) A paired-end sequencing strategy to map the complex landscape of transcription initiation. Nat Methods 7(7):521–527

Olivier N, Cédric C, Martin-Garin B, Lathuilière B, Gaillard C, Ferry S, Hantzpergue P, Geister J (2004) Coral-microbialite reefs in pure carbonate versus mixed carbonate-siliciclastic depositional

environments: the example of the Pagny-sur-Meuse section (Upper Jurassic, northeastern France). Facies 50(2):229–255
Pederson CL, Mcneill DF, Klaus JS, Swart PK (2015) Deposition and diagenesis of marine oncoids: implications for development of carbonate porosity. J Sediment Res 85:1323–1333
Peng SC, Zhao YL (2018) The proposed global standard stratotype-section and point (GSSP) for the conterminous base of Miaolingian series and Wuliuan stage at Balang, Jianhe, Guizhou, China was ratified by IUGS. J Stratigr 42(3):325–327 (in Chinese without English abstract)
Peryt TM (1981) Phanerozoic oncoids: an overview. Facies 4:197–214
Peters SE, Gaines RR (2012) Formation of the 'Great Unconformity' as a trigger for the Cambrian explosion. Nature 484:363–366
Peters SE, Husson JM, Wilcots J (2017) The rise and fall of stromatolites in shallow marine environments. Geology 45:487–490
Pratt BR, Raviolo MM, Bordonaro OL (2012) Carbonate platform dominated by peloidal sands: lower Ordovician La Silla Formation of the eastern Precordillera, San Juan, Argentina. Sedimentology 59:843–866
Qi YA, Chai S, Zhang XY, Dai MY, Wang M (2016) Oncoids and their depositional features from the second member of Mantou Formation (Cambrian Series 3), Weihui area, Henan Province. China Science paper, 21(11): 2416–2421. (in Chinese with English abstract).
Rees MN, Pratt BR, Rowell AJ (1989) Early Cambrian reefs, reef complexes, and associated lithofacies of the Shackleton Limestone, Transantarctic Mountains. Sedimentology 36:341–361
Reitner J (2011a) Microbial Mats. In: Reitner J, Thiel V (eds) Encyclopedia of geobiology. Springer, Berlin, pp 606–608
Reitner J (2011b) Biofilm. In: Reitner J, Thiel V (eds) Encyclopedia of geobiology. Springer, Berlin, pp 134–135
Riaz M (2019) Integrated sedimentology and sequence stratigraphy of the Cambrian ooids in the North China Platform. Dissertation, China University of Geosciences, Beijing
Riaz M, Latif K, Zafar T, Xiao EZ, Ghazi S, Wang L, Hussein AAA (2019a) Assessment of Cambrian sequence stratigraphic style of the North China Platform exposed in Wuhai division, Inner Mongolia. Himal Geol 40(1):92–102
Riaz M, Xiao EZ, Latif K, Zafar T (2019b) Sequence-stratigraphic position of oolitic bank of Cambrian in North China Platform: Example from the Kelan section of Shanxi Province. Arab J Sci Eng 44(1): 391–407
Riding R (1991) Calcified cyanobacteria. In: Riding R (ed) Calcareous algae and stromatolites. Springer, Berlin, pp 55–87
Riding R (2000) Microbial carbonates: the geological record of calcified bacterial-algal mats and biofilms. Sedimentology 47:179–214
Riding R (2011a) Microbialites, stromatolites, and thrombolites. In: Reitner J, Thiel V (eds) Encyclopedia of Geobiology. Springer, Berlin, pp 635–654
Riding R (2011b) Calcified cyanobacteria. In: Reitner J, Thiel V (eds) Encyclopedia of geobiology. Springer, Heidelberg, pp 211–223
Rimmer SM (2004) Geochemical paleoredox indicators in Devonian–Mississippian black shales, Central Appalachian Basin (USA). Chem Geol 206:373–391
Samanta P, Mukhopadhyay S, Eriksson PG (2016) Forced regressive wedge in the Mesoproterozoic Koldaha shale, Vindhyan basin, Son Valley, central India. Mar Pet Geol 71:329–343
Schaefer MO, Gutzmer J, Beukes NJ (2001) Late Paleoproterozoic Mn-rich oncoids: earliest evidence for microbially mediated Mn precipitation. Geology 29(9):835–838
Schinder E (2012) "Time-specific facies" – a great concept introduced by a great man: Otto H. Walliser. Palaeogeogr Palaeocl 367–368:3–5
Schlager W (1989) Drowning unconformities on carbonate platforms. In: Crevello PD, Wilson JL, Sarg JF, Read JF (eds) Controls on carbonate platform and basin development. SEPM Spe Pub 44: pp 15–25
Schlager W (1998) Exposure, drowning and sequence boundaries on carbonate platforms. In: Camoin G, Davies P (eds) Reefs and carbonate platforms in the Pacific and Indian oceans. Int As Sed 25: pp 3–21
Schlager W (1999) Type 3 sequence boundaries. In: Harris P, Saller A, Simo A (eds) Carbonate sequence stratigraphy: application to reservoirs, outcrops and models. SEPM Spe Pub 63: pp 35–46
Schlager W, Warrlich G (2009) Record of sea-level fall in tropical carbonates. Basin Res 21(2):209–224
Sen S, Mishra M (2015) Geochemistry of Rohtas limestone from Vindhyan Supergroup, Central India: evidences of detrital input from felsic source. Geochem Int 53(12):1107–1122
Sholkovitz ER (1990) Rare earth elements in marine sediments and geochemical standards. Chem Geol 88:333–347
Soule T, Palmer K, Gao Q, Potrafka RM, Stout V, Garcia-Pichel F (2009) A comparative genomics approach to understanding the biosynthesis of the sunscreen scytonemin in cyanobacteria. BMC Genomics 10:336–345
Stanley SM (2006) Influence of seawater chemistry on biomineralization throughout Phanerozoic time: paleontological and experimental evidence. Palaeogeogr Palaeocl 232:214–236
Tobia FH (2018) Stable isotope and rare earth element geochemistry of the Baluti carbonates (Upper Triassic), Northern Iraq. Geosci J 22(6):975–987
Tourney J, Ngwenya BT (2014) The role of bacterial extracellular polymeric substances in geomicrobiology. Chem Geol 386:115–132
Tripati AK, Allmon WD, Sampson DE (2009) Possible evidence for a large decrease in seawater strontium/calcium ratios and strontium concentrations during the Cenozoic. Earth Planet Sci Lett 282(1): 122–130
Vedrine S, Strasser A, Hug W (2007) Oncoid growth and distribution controlled by sea-level fluctuations and climate (Late Oxfordian, Swiss Jura Mountains). Facies 53:535–552
Wang H, Xiao EZ (2018) Oncolites in Cambrian Series 3 at Diaoquan section in Lingqiu. Shanxi. J Northeast Petrol Univ 42(5):44–53. (in Chinese with English abstract)
Wotte T, Álvaro JJ, Shields GA, Brown B, Brasier MD, Veizer J (2007) C-, O- and Sr-isotope stratigraphy across the Lower-Middle Cambrian transition of the Cantabrian Zone (Spain) and the Montagne Noire (France), West Gondwana. Palaeogeogr Palaeoclimatol Palaeoecol 256:47–70
Xiao EZ, Zafar T, Latif K, Riaz M, Lu Y (2020a) Geochemical and petrographic analyses of the Cambrian oncoids of the North China platform: implications for their paleogeography and paleoenvironment. Arab J Sci Eng 45(1):307–325
Xiao EZ, Mei MX, Jiang S, Zafar T (2020b) Morphology and features of Cambrian oncoids and responses to palaeogeography of the North China Platform. J Palaeogeogr 9(7). https://doi.org/10.1186/s42501-020-0055-1
Yang R, Fan A, Han Z, Chai N (2011) Status and prospect of studies on oncoid. Adv Earth Science 26:465–474 (in Chinese with English abstract)
Zhang KM, Huang WH, Wang JH (2013) Characteristics and Environmental Significance of Lacustrine Oncolites in Paleogene Guanzhuang Formation in Pingyi Basin, Shandong Province in Eastern China. Acta Sedimentol Sin 31(2):259–268 (in Chinese with English abstract)
Zhang WH, Shi XY, Tang DJ, Jiang GQ (2014a) Oncolites from lower-middle Cambrian transition of the western north china platform: a study of their ultra-fabrics and biomineralization. Geoscience 28(1): 1–15 (in Chinese with English abstract)
Zhang WH, Shi XY, Tang DJ, Wang X (2014b) Mass-occurrence of oncoids in the early-middle Cambrian transition at the western margin of north china platform: a response of microbial community to shallow marine anoxia. J Palaeogeogr 16(3):305–318 (in Chinese with English abstract)

Zhang W, Shi X, Jiang G, Tang D, Wang X (2015a) Mass-occurrence of oncoids at the Cambrian Series 2–Series 3 transition: implications for microbial resurgence following an early Cambrian extinction. Gondwana Res 28(1):432–450

Zhang XY, Qi YA, Dai M, Chai S (2015b) Coupling variation of oncoids and trace fossils in the Zhangxia Formation (Cambrian Series 3), Dengfeng, western Henan province. Acta Micropalaeontol Sin 32(2):184–193 (in Chinese with English abstract)

Zheng YF, Xiao WJ, Zhao G (2013) Introduction to tectonics of China. Gondwana Res 23:1189–1206

Zhou G, Zheng R, Zhao G (2017) Characteristics, Origin and Geological Significance of Oncoids of Givetian (Middle Devonian) in Ganxi Area, Northwestern Sichuan. J Jilin Uni 47(2):405–417 (in Chinese with English abstract)

Affiliations

Muhammad Riaz[1,2,3] · Tehseen Zafar[4] · Khalid Latif[5,6] · Shahid Ghazi[3] · Enzhao Xiao[6]

1 State Key Laboratory of Oil and Gas Reservoir Geology and Exploitation, Chengdu University of Technology, Chengdu 610059, China

2 College of Energy Resources, Chengdu University of Technology, Chengdu 610059, China

3 Institute of Geology, University of the Punjab, Lahore 54590, Pakistan

4 Institute of Geochemistry, Chinese Academy of Sciences, Guiyang 550081, China

5 National Centre of Excellence in Geology, University of Peshawar, Peshawar 25130, Pakistan

6 School of Earth Sciences and Resources, China University of Geosciences, Beijing 100083, China